Comprehensive Rock Engineering (TA706/C642) Ref.
Ed. Hudson J.A, Brown E.T., Fairhurst C. and Hoek, E., chap 13, Vol. 2. Pregamon, Oxford (1993).

3

Numerical Modeling of Yield Zones in Weak Rock

MARY E. DUNCAN FAMA
CSIRO, Kenmore, Queensland, Australia

3.1 INTRODUCTION 49
3.1.1 Preliminary Remarks 49
3.1.2 Plasticity Theories 50
3.2 DEFORMATION THEORY OF PLASTICITY 51
3.2.1 Definition of the Excavation Unloading Plane Strain Boundary Value Problem of Geomechanics 52
3.2.2 Definition of Secant Modulus for Plane Strain 53
3.2.3 Mohr–Coulomb Failure Criterion 54
3.2.4 Strain-softening 54
3.2.5 Application to Finite Element Calculations and Determination of Secant Modulus 55
3.3 AXISYMMETRIC PROBLEMS 56
3.3.1 Mohr–Coulomb Yield Zone Stresses 56
3.3.2 Deformation Theory Constitutive Relations for Axisymmetry 57
3.3.3 Analytical Solutions for Displacements 58
3.3.3.1 No strain-softening 58
3.3.3.2 Simplest approximation for strain-softening 59
3.3.3.3 Analytical solution for a smooth cohesion reduction in the yield zone 59
3.3.3.4 Approximation for λ in deformation theory 62
3.4 PLANE STRAIN PROBLEMS FOR CIRCULAR EXCAVATIONS 63
3.5 APPLICATION TO UNDERGROUND COAL MINING IN AUSTRALIA 67
3.6 THE IMPORTANCE OF THE PSEUDO *IN SITU* STRESS 72
3.7 CONCLUSION 73
3.8 APPENDIX: SOLUTION FOR AN ELASTIC RING BONDED TO A SEMIINFINITE MEDIUM 74
3.9 REFERENCES 75

3.1 INTRODUCTION

3.1.1 Preliminary Remarks

It is a common practice in numerical modeling of geological materials to assume that weakened or partly fractured materials can be modeled by a linear elastic material with a low modulus of elasticity. An extreme example is a coal mine goaf where the modulus is often assumed to be of the order of one-tenth or less of the coal or roof material (*e.g.* Trueman [1]). The motivation behind this procedure is obvious. Such materials are highly deformable and their response to load is similar to that of a low-modulus medium. Often, not enough is known of their properties to justify an elastic-plastic analysis. The latter also consumes a lot of computer time and resources.

It is the purpose of this chapter to show that the above procedure fits within the framework of the deformation theory of plasticity (see for example, Vermeer [2]). However, an important addition to

present practice needs to be made to conform to the principles of the deformation theory. This addition is that the initial or *in situ* stress unloaded from such a weakened material to model the formation of an excavation must be reduced also. This concept will be explained in detail in Section 3.2.

The major difficulty in the numerical modeling of geological materials is in the determination of the input parameters. Results of laboratory tests for such parameters as the modulus of elasticity and Mohr–Coulomb or Hoek–Brown failure properties are not always relevant to the rock *in situ*. Attempts have been made to overcome these problems by the scaling of input parameters, *e.g.* Wilson [3], and Rock Mass Classification schemes, described in Hoek and Brown [4], have also been used to infer input parameters relevant to *in situ* conditions (*e.g.* Bieniawski [5], Follington and Isaac [6]).

An alternative approach is the use of back-analysis (*e.g.* Sakurai [7]). For large projects, usually in civil not mining engineering, pilot tunnels are driven and displacements and stresses are extensively monitored. Back-analysis techniques have been developed to infer from the results of these measurements the input parameters for numerical models. Weakened regions are modeled by material of lower modulus than the intact medium. Thus the work described in this chapter is relevant to this type of analysis also. It will be shown that the results obtained from back-analysis can conform to a conventional plasticity theory provided the reduced *in situ* stress mentioned above is used.

It will be shown in the chapter that equivalent elastic properties of a weakened or yielded rock can be related, *via* the deformation theory of plasticity, to failure and postfailure properties, such as pre- and post-failure cohesion and angle of friction, of the rock.

A major advantage of the deformation theory description adopted here is ease of computation. The formulation is done in such a way that an iterative procedure can be set up with a linear elastic finite element program.

3.1.2 Plasticity Theories

A detailed description of plasticity theory will not be given here. The reader is referred to text books such as Hill [8] or Kachanov [9]. What is of concern is the difference between the so-called incremental theories of plasticity and the deformation theories. The discussion will be in terms of the reduction of tractions on the boundary of an excavation in a rock, rather than the application of load to a finite body as occurs in laboratory tests or in many civil and mechanical engineering applications where structures are made above ground. Before the excavation takes place, tractions on the excavation boundary are in equilibrium with the *in situ* stresses in the rock, and they must be reduced to zero for an unsupported opening or to some nonzero values which represent the support loads. If the material is linear elastic, it is well known that the final state of stress is obtained by the solution to the boundary value problem in which the support pressure is applied to the opening boundary and the tractions resulting from the *in situ* stresses are applied to a boundary far away from the opening. The boundary value problem for the displacements induced by the excavation is described in detail in Section 3.2.1.

The essential difference between the two plasticity theories is as follows. The deformation theory of plasticity, originally due to Hencky [10], uses the same boundary conditions as the linear elastic problem to be described in Section 3.2.1. However, the stresses are constrained to satisfy a yield criterion (usually Mohr–Coulomb or Hoek–Brown for geomechanics applications). Where the material has yielded, (*i.e.* this criterion has been violated at some stage of the solution process), the strains are related to the stresses by a constitutive equation which is no longer the linear elastic Hooke's law. This constitutive equation, however, like Hooke's law, does relate the final induced strains to the difference between the final stresses and the initial stresses. In its simplest form, the deformation theory describes a linear elastic inhomogeneous material, because the secant modulus of elasticity varies from point to point in the medium.

In contrast, in the incremental theories, the boundary tractions are reduced in increments until the material adjacent to the opening yields. Further increments of stress occasioned by further reductions in traction are distributed to neighboring elements which may yield in turn. The constitutive equations in yielded elements relate the increment of strain to the increment of stress.

In summary, the incremental theories attempt to follow the path of loading and unloading in an element of material, whereas the deformation theories describe only the final state of the material. In cases of complicated loading paths (including any unloading) the resulting state is known to be path dependent and the deformation theories are inapplicable. For this reason, the deformation theories

were discredited in the 1950s. However, Sanders [11] proved that the incremental theory is integrable, for linear yield surfaces. Budiansky [12] showed further that, for some restricted loading paths (not too far from proportional loading), the incremental theories are in effect integrable and give identical results to the corresponding deformation theory. Thus, in the absence of strain-softening, for a single unsupported excavation in a homogeneous medium where the stresses are limited by a Mohr–Coulomb criterion and the plastic strains obey an associated flow law, the deformation theory gives the same results as the incremental theory. This fact is not widely known in the geomechanics community.

For a Mohr–Coulomb failure criterion, this result has been confirmed for circular excavations under nonaxisymmetric *in situ* stresses, if the obliquity (defined below) of these stresses is not too great [13]. The flow rule does not need to be an associated one. In this chapter we demonstrate Sanders' theorem numerically, by showing that, for circular excavations in plane strain conditions, the departure from axisymmetry can be greater yet and again the flow rule does not need to be associated. We also give a similar example with strain-softening, where the incremental theory and the deformation theory give virtually identical results.

There are instances of deformation theory applied to geomechanics problems recently in the literature, see refs. 2 and 14.

In many instances of underground excavation there is very little of the complicated sequence of loading and unloading which makes the use of incremental theory mandatory. Moreover, even though we may simulate the path of excavation unloading as convincingly as we can, it is not clear that the path we choose, mathematically, is actually the path that elements of the material follow! When a continuous miner cuts a roadway in coal it is reasonable to assume that a couple of roadway diameters from the face end we have plane strain conditions. To say that the traction on the roadway perimeter has reduced smoothly from its original *in situ* value to zero in small steps of equal magnitude (in plane strain) is not necessarily an accurate description of the complicated three-dimensional effects as the face advances. Thus the results of a deformation theory analysis may reflect the true situation just as adequately as an incremental theory analysis.

3.2 DEFORMATION THEORY OF PLASTICITY

As with the incremental theory of plasticity, the deformation theory splits the infinitesimal strain tensor ε_{ij} into an elastic part ε^e_{ij} and a plastic part ε^p_{ij}.

The elastic part of the strain tensor is related to the Cauchy stress tensor σ_{ij} by the usual generalized linear Hooke's law as follows

$$E\varepsilon^e_{ij} = (1 + \nu)\sigma_{ij} - \nu\sigma_{kk}\delta_{ij} \tag{1}$$

Here E is the modulus of elasticity and ν the Poisson's ratio of the medium. Note that ν is constant throughout the analysis.

The plastic part of the strain tensor is split into deviatoric e^p_{ij} and volumetric ε^p_{kk} parts

$$\varepsilon^p_{ij} = e^p_{ij} + (\varepsilon^p_{kk}/3)\delta_{ij} \tag{2}$$

The deformation theory constitutive relations for plastic strain are taken in the form

$$E^* e^p_{ij} = (1 + \nu)s_{ij} \tag{3}$$

and

$$\varepsilon^p_{kk} = D(\gamma^p) \tag{4}$$

where the stress deviator s_{ij} is defined by

$$s_{ij} = \sigma_{ij} - (\sigma_{kk}/3)\delta_{ij} \tag{5}$$

and where E^* is a function of the invariants of σ_{ij}, γ^p, the total plastic strain, is defined below in equation (16) and $D(\gamma^p)$ is a function of γ^p yet to be defined. (For example the so-called J_2 deformation theory assumes that $E^*/(1 + \nu) = 2G^*$ is a function of the second invariant $J_2 = s_{ij}s_{ij}/2$ only and that $D \equiv 0$.) For more details on the deformation theory the reader is referred to textbooks such as Kachanov [9].

We note that the analysis in this chapter will be confined to small displacements and small strains, so that the strains arise from displacements according to the linear strain–displacement relations

$$\varepsilon_{ij} = (u_{i,j} + u_{j,i})/2 \tag{6}$$

In Section 3.2.1 the boundary value problem will be described that simulates the formation of an excavation in rock. The discussion will be restricted to two-dimensional plane strain problems. Then in Section 3.2.2 the deformation theory constitutive equations for plane strain are written out in cartesian components. Because these constitutive equations are not in a convenient form for computation, they are recast so that they describe a linear elastic inhomogeneous medium with varying secant modulus subject to a 'pseudo' *in situ* stress field (which will be defined) which also varies in the medium. It then becomes a simple matter to set up an iterative procedure with a linear elastic finite element program to produce a solution.

In what follows we put $x_1 = x$, $x_2 = y$ and $x_3 = z$, $\sigma_{11} = \sigma_x$, $\sigma_{12} = \sigma_{xy}$, $\sigma_{22} = \sigma_y$ *etc.* Einstein's summation convention ($i, j = 1, 2$) is implied by a repeated index and $_{,j} = \partial/\partial x_j$.

3.2.1 Definition of the Excavation Unloading Plane Strain Boundary Value Problem of Geomechanics

Consider an 'infinite medium' subjected to *in situ* stresses σ_x^0, σ_y^0 and σ_{xy}^0 in the x, y plane and with zero strain, ε_z, normal to the plane. If a single excavation of any constant shape is made parallel to the z direction (a tunnel or borehole), the stresses around the excavation will be modified and displacements and strains will be induced there.

This procedure is modeled mathematically by reducing the normal and tangential tractions on the boundary of the excavation from their *in situ* values to values appropriate to any support there or to zero. In the incremental theories of plasticity, these tractions will be reduced gradually (in increments) until the rock around the opening yields. The process will be continued with stress redistribution taking place in and around the yielded rock until the final boundary values are reached. For the deformation theory of plasticity the boundary value problem is not solved in increments but the final values are applied at once. However, an iterative process is required to ensure that the deformation theory constitutive equations are satisfied.

The unusual feature of the geomechanics 'excavation unloading' boundary value problem is apparent when we discuss the appropriate boundary conditions.

Suppose that S is the closed curve that is the boundary of the excavation, n_i are the direction cosines of the normal to S and T_i are tractions on S arising from supports.

If the finite element method is to be used to solve a problem, an outer boundary S_0 must be introduced far from the excavation. The solution to the problem must satisfy the conditions that $\sigma_{ij}n_j = T_i$ on S as well as $\sigma_{ij} \to \sigma_{ij}^0$ and the displacements $u_i \to 0$ as the field point $x_i \to$ a point on S_0.

The solution cannot be obtained by simply applying boundary conditions $\sigma_{ij} = \sigma_{ij}^0$ on S_0 and $\sigma_{ij}n_j = T_i$ on S, for clearly this will induce displacements on S_0. This boundary value problem is termed the 'outer boundary loading problem' and is still widely used in geomechanics.

To get a solution where the displacements and induced strains arise only from the introduction of the excavation, we solve for stresses $\Delta\sigma_{ij} = \sigma_{ij} - \sigma_{ij}^0$ which satisfy the following boundary conditions: (i) $\Delta\sigma_{ij}n_j = -\sigma_{ij}^0 n_j + T_i$ on S; and (ii) $\Delta\sigma_{ij}n_j = 0$ (so that $u_i \approx 0$) on S_0 or $u_i = 0$ (so that $\Delta\sigma_{ij}n_j \approx 0$) on S_0.

The stresses, $\Delta\sigma_{ij}$, must satisfy the equilibrium equations

$$\Delta\sigma_{ij,j} + f_i = 0 \tag{7}$$

(where f_i are body forces), and the constitutive equations (1), (3) and (4) with σ_{ij}, (σ_{kk}) replaced by $\Delta\sigma_{ij}$, $(\Delta\sigma_{kk})$.

The final stresses σ_{ij} are obtained from the solution stresses $\Delta\sigma_{ij}$ by adding the *in situ* stresses σ_{ij}^0. It is clear that σ_{ij} approach the *in situ* stresses σ_{ij}^0 far away from the excavation and satisfy the support conditions around the excavation. It is these final stresses σ_{ij} that are to be constrained to satisfy the yield condition described below.

3.2.2 Definition of Secant Modulus for Plane Strain

For plane strain ($\varepsilon_z^e = \varepsilon_z^p = 0$), the elastic stress–strain relations are

$$\varepsilon_x^e = \frac{1+\nu}{E}[(1-\nu)\Delta\sigma_x - \nu\Delta\sigma_y] \tag{8a}$$

$$\varepsilon_y^e = \frac{1+\nu}{E}[(1-\nu)\Delta\sigma_y - \nu\Delta\sigma_x] \tag{8b}$$

$$\varepsilon_{xy}^e = \frac{1+\nu}{E}\Delta\sigma_{xy} \tag{8c}$$

In two dimensions the deviatoric parts of the stress and plastic strain tensor are defined as

$$\varepsilon_{ij}^p = e_{ij}^p + (\varepsilon_{kk}^p/2)\delta_{ij} \tag{9}$$

$$s_{ij} = \sigma_{ij} - (\sigma_{kk}/2)\delta_{ij} \tag{10}$$

so that

$$s_x = (\sigma_x - \sigma_y)/2 \tag{11a}$$

$$s_y = -(\sigma_x - \sigma_y)/2 \tag{11b}$$

Then the full stress–strain relations for the deformation theory in cartesian coordinates x and y, using equations (8), (3) and (4), are as follows

$$\begin{aligned}\varepsilon_x &= \varepsilon_x^e + \varepsilon_x^p \\ &= \frac{1+\nu}{E}[(1-\nu)\Delta\sigma_x - \nu\Delta\sigma_y] + \frac{1+\nu}{E^*}(\sigma_x - \sigma_y)/2 + D(\gamma^p)/2\end{aligned} \tag{12a}$$

$$\begin{aligned}\varepsilon_y &= \varepsilon_y^e + \varepsilon_y^p \\ &= \frac{1+\nu}{E}[(1-\nu)\Delta\sigma_y - \nu\Delta\sigma_x] - \frac{1+\nu}{E^*}(\sigma_x - \sigma_y)/2 + D(\gamma^p)/2\end{aligned} \tag{12b}$$

$$\begin{aligned}\varepsilon_{xy} &= \varepsilon_{xy}^e + \varepsilon_{xy}^p \\ &= \frac{1+\nu}{E}\Delta\sigma_{xy} + \frac{1+\nu}{E^*}\sigma_{xy}\end{aligned} \tag{12c}$$

The above equations are not in a convenient form for computation. Noting, however, that finite element software easily calculates nodal forces corresponding to nonuniform initial or *in situ* stresses in elements with different values of modulus of elasticity, we seek to recast the constitutive equations (12a–c) in the following form

$$\varepsilon_x = \frac{1+\nu}{E_s}[(1-\nu)\Delta_\lambda\sigma_x - \nu\Delta_\lambda\sigma_y] \tag{13a}$$

$$\varepsilon_y = \frac{1+\nu}{E_s}[(1-\nu)\Delta_\lambda\sigma_y - \nu\Delta_\lambda\sigma_x] \tag{13b}$$

$$\varepsilon_{xy} = \frac{1+\nu}{E_s}\Delta_\lambda\sigma_{xy} \tag{13c}$$

where

$$\Delta_\lambda\sigma_{ij} = \sigma_{ij} - \lambda_{(ij)}\sigma_{ij}^0 \tag{14}$$

(where (ij) denotes that i, j are not summed). Equations (12a–c) and (13a–c) are identical provided

$$1/E_s = 1/E + 1/E^* \tag{15a}$$

$$\lambda_x\sigma_x^0 = (E_s/E)\sigma_x^0 + (1 - E_s/E)(\sigma_x + \sigma_y)/2 - E_sD(\gamma^p)/[2(1 + \nu)(1 - 2\nu)] \tag{15b}$$

$$\lambda_y\sigma_y^0 = (E_s/E)\sigma_y^0 + (1 - E_s/E)(\sigma_x + \sigma_y)/2 - E_sD(\gamma^p)/[2(1 + \nu)(1 - 2\nu)] \tag{15c}$$

$$\lambda_{xy}\sigma_{xy}^0 = (E_s/E)\sigma_{xy}^0 \tag{15d}$$

γ^p, the total plastic strain, is given by

$$\gamma^p = \varepsilon_1^p - \varepsilon_3^p = [(\varepsilon_x^p - \varepsilon_y^p)^2 + 4\varepsilon_{xy}^{p2}]^{1/2} \tag{16}$$

where ε_1^p, ε_3^p are respectively the major and minor principal plastic strains. Note that γ^p is often defined as a half of the above. Similarly, the shear stress τ is given by

$$\tau = (\sigma_1 - \sigma_3)/2 = [(\sigma_x - \sigma_y)^2/4 + \sigma_{xy}^2]^{1/2} \tag{17}$$

where σ_1, σ_3 are respectively the major and minor principal stresses. Then, using equations (3), (10) and (11) with equation (15a) we have

$$\gamma^p = 2(1 + \nu)(1/E^*)\tau = 2(1 + \nu)(1/E_s - 1/E)\tau \tag{18}$$

Equations (13a–c) describe a linear elastic inhomogeneous medium with varying secant modulus E_s and subject to a pseudo *in situ* stress field $\lambda_x\sigma_x^0$, $\lambda_y\sigma_y^0$ and $\lambda_{xy}\sigma_{xy}^0$ which also varies in the medium.

3.2.3 Mohr–Coulomb Failure Criterion

We postulate that the rock obeys a Mohr–Coulomb failure criterion

$$\sigma_1 = k\sigma_3 + \sigma_c \tag{19}$$

where σ_1 and σ_3 are respectively the major and minor principal stresses in the x, y plane, σ_c is the unconfined compressive strength of the rock and k (triaxial strength) is related to the angle of internal friction (ϕ) of the rock

$$k = (1 + \sin\phi)/(1 - \sin\phi) \tag{20}$$

The cohesion c of the rock is related to σ_c and ϕ by the following

$$c = \sigma_c\tan\phi/(k - 1) \tag{21}$$

It is assumed that the stress in the z direction is a principal stress and is intermediate in value between σ_1 and σ_3. It is further assumed that σ_3 is limited by a maximum value for tension.

3.2.4 Strain-softening

For many geological materials, the effective cohesion or unconfined compressive strength is much less after yield has occurred. The crudest way to account for this is simply to reduce the cohesion in the yield zone to a constant value. Naturally, a continuous drop in cohesion from pre- to post-failure is preferred and several ways of doing this have been proposed (see Brown *et al.* [15] for a review). Normally, the cohesion reduction is given as a function of γ^p, the total plastic strain (equation 16).

The following expression has been adopted to fit the framework of the deformation theory constitutive equations described here. If σ_c' is the limiting value of unconfined compressive strength in the yield zone as $E_s \to 0$, we replace equation (19) in yielded elements by

$$\sigma_1 = k\sigma_3 + \sigma_c^* \tag{22}$$

where

$$\sigma_c^* = \sigma_c - [1 - (E_s/E)^a](\sigma_c - \sigma_c') \tag{23}$$

for some constant α. Note that this gives a smooth variation of σ_c^* from σ_c on the yield–elastic zone interface (where $E_s = E$), to σ_c' as $E_s \to 0$.

3.2.5 Application to Finite Element Calculations and Determination of Secant Modulus

In what follows the plastic region will normally be termed the yield zone.

For finite element calculations equations (13a–c) allow an iterative procedure to be set up where each iteration is a linear elastic analysis with: (i) the modulus of elasticity in each element of the plastic region equal to the current estimate of the secant modulus in that element (the Poisson's ratio, ν, is assumed to be constant for each iteration); and (ii) the nodal forces calculated from the pseudo *in situ* stress field $\lambda_x\sigma_x^0$, $\lambda_y\sigma_y^0$ and $\lambda_{xy}\sigma_{xy}^0$, which also depend on the current secant modulus and the current stress state.

The first iteration is a linear elastic analysis with the original measured or inferred Young's modulus in the different strata around the excavation and the full *in situ* stress unloaded at the excavation boundary (*i.e.* all the $\lambda_{ij} = 1$). Each finite element is then tested to see whether the stress in that element predicted by the analysis violates the Mohr–Coulomb failure criterion postulated for that material. If this criterion is violated, the element is flagged as 'yielded', and the secant modulus for the element for the next iteration is obtained by multiplying the appropriate Young's modulus by a reduction factor, F_{os}, defined below. The factors λ_x, λ_y and λ_{xy} are then computed for this secant modulus using the stress state from this iteration. Nodal forces are calculated as described in (ii) above and a new iteration performed. The procedure is continued for each iteration until the reduction factors, F_{os}, are close enough to unity (usually within 1%).

The reduction factors are obtained from the following analysis.

From equations (13a–c) and using equations (14) and (15), we derive

$$\varepsilon_x - \varepsilon_y = \frac{1+\nu}{E_s}[\sigma_x - \sigma_y - (\lambda_x\sigma_x^0 - \lambda_y\sigma_y^0)] \tag{24a}$$

$$= \frac{1+\nu}{E_s}[\sigma_x - \sigma_y - (E_s/E)(\sigma_x^0 - \sigma_y^0)] \tag{24b}$$

$$= \frac{1+\nu}{E_s}(\sigma_x - \sigma_y) - \frac{1+\nu}{E}(\sigma_x^0 - \sigma_y^0) \tag{24c}$$

If E_i is the modulus of elasticity estimate for the ith iteration then the stresses computed at the end of the ith iteration satisfy

$$\begin{aligned} \sigma_x - \sigma_y &= [E_i/(1+\nu)][(\varepsilon_x + \varepsilon_x^0) - (\varepsilon_y + \varepsilon_y^0)] \\ \sigma_{xy} &= [E_i/(1+\nu)](\varepsilon_{xy} + \varepsilon_{xy}^0) \end{aligned} \tag{25}$$

where we have defined

$$\varepsilon_x^0 = \frac{1+\nu}{E}\sigma_x^0 \tag{26a}$$

$$\varepsilon_y^0 = \frac{1+\nu}{E}\sigma_y^0 \tag{26b}$$

$$\varepsilon_{xy}^0 = \frac{1+\nu}{E}\sigma_{xy}^0 \tag{26c}$$

Thus the shear stress τ (equation 17) satisfies

$$\tau = \gamma_{i0}E_i/[2(1+\nu)] \tag{27}$$

where

$$\gamma_{i0}^2 = [(\varepsilon_x + \varepsilon_x^0) - (\varepsilon_y + \varepsilon_y^0)]^2 + 4(\varepsilon_{xy} + \varepsilon_{xy}^0)^2 \tag{28}$$

σ_1 is supposed to satisfy the postfailure yield criterion, equation (22). Thus

$$\tau_{\text{required}} = [(\sigma_1 - \sigma_3)/2]_{\text{required}} = [(k-1)\sigma_3 + \sigma_c^*]/2 \tag{29}$$

Referring to equation (27), let us choose E_{i+1} to satisfy

$$\begin{aligned} E_{i+1} &= 2(1+\nu)\tau_{\text{required}}/(\gamma_{i0}) \\ &= \tau_{\text{required}}/[\tau_{\text{computed}}/E_i] \\ &= E_i[(k-1)\sigma_3 + \sigma_c^*]/[\sigma_1 - \sigma_3] \end{aligned} \tag{30}$$

Hence

$$E_{i+1} = F_{os}E_i \tag{31}$$

where

$$F_{os} = [(k-1)\sigma_3 + \sigma_c^*]/[\sigma_1 - \sigma_3] \tag{32}$$

The reduction factor F_{os} is the same as that used previously by Kripakov and Melvin [16] and Duncan Fama [17] to reduce the modulus of elasticity in yielded regions. (The term reduction factor is preferred rather than factor of safety, in case of confusion with a design factor of safety.) The iterative procedure has been found to converge extremely well for many problems. Oscillations may occur, but the procedure can be tuned when this happens (*e.g.* by using $F_{os}^{1/2}$ instead of F_{os} in equation 31). The calculation of the nodal forces from a pseudo *in situ* stress field for excavation unloading is believed to be new.

The procedure is implemented in a two-dimensional plane strain finite element program, FESOFT (© CSIRO).

3.3 AXISYMMETRIC PROBLEMS

For axisymmetric plane strain problems (circular tunnels or boreholes), the incremental theories of plasticity are always integrable because the loading path is proportional. Thus a deformation theory gives the same answer as an incremental theory provided unloading does not occur.

In this section some useful results for axisymmetric plane strain strain-softening problems are derived. Firstly, in Section 3.3.1 the well-known ideal plasticity solution for the stresses is presented and equation (46) for λ relevant to axisymmetry is given.

Although equation (46) looks unpleasant, the stress–strain equations (40a–c) can be solved analytically, both for the case of ideal plasticity, and also for the case where the failure properties are reduced to a constant in the yield zone. See, for example, Brown *et al.* [15] for a review of where such solutions are to be found. These authors also gave a solution appropriate to the Hoek–Brown failure criterion (assuming a constant elastic strain in the yield zone). The analytical solutions for displacements, total plastic strain and secant modulus for the ideal plasticity case are presented in Section 3.3.3.1. In Section 3.3.3.2, a solution for the Mohr–Coulomb failure criterion, with a constant reduced cohesion in the yield zone, is presented. The latter is a simplification of the deformation theory solution. In Section 3.3.3.3, postulating that cohesion softening is proportional to confinement, allows an analytical solution for both stresses and displacements to be obtained from the ideal plasticity solution. Finally, in Section 3.3.3.4 an approximate expression for λ allows a particularly simple analytical solution for the displacements to be obtained.

3.3.1 Mohr–Coulomb Yield Zone Stresses

For a circular tunnel (or borehole) in homogeneous isotropic rock under hydrostatic pressure, p_0, the *in situ* stresses are given by $\sigma_x^0 = \sigma_y^0 = p_0$ with $\sigma_{xy}^0 = 0$. Defining polar coordinates r, θ in the usual way, if r_i is the radius of the circular excavation, and $p_i < p_0$ the (support) pressure there, then the stresses in the elastic region have $\sigma_\theta > \sigma_r$ everywhere. Thus the major principal stress σ_1 is σ_θ, and the minor principal stress is σ_r. The Mohr–Coulomb failure criterion (equation 19) becomes

$$\sigma_\theta = k\sigma_r + \sigma_c \tag{33}$$

which is linear in the stresses, and it is well known that the stresses in the yield zone are now statically determined by this equation in combination with the usual equilibrium equation in polar

coordinates

$$\frac{d\sigma_r}{dr} = (\sigma_\theta - \sigma_r)/r \tag{34}$$

If r_e is the radius and p_e the normal stress at the yield–elastic zone interface, then the stresses in the elastic region $r \geq r_e$ are

$$\sigma_r = p_0 - (p_0 - p_e)\left[\frac{r_e}{r}\right]^2 \tag{35a}$$

$$\sigma_\theta = p_0 + (p_0 - p_e)\left[\frac{r_e}{r}\right]^2 \tag{35b}$$

$$\sigma_{r\theta} = 0 \tag{35c}$$

and the stresses in the yield zone $r \leq r_e$ are

$$\sigma_r = (p_i + s)\left[\frac{r}{r_i}\right]^{k-1} - s \tag{36a}$$

$$\sigma_\theta = k(p_i + s)\left[\frac{r}{r_i}\right]^{k-1} - s \tag{36b}$$

$$\sigma_{r\theta} = 0 \tag{36c}$$

where

$$s = \frac{\sigma_c}{k-1} \tag{37}$$

Continuity of the radial and tangential stress at the yield–elastic interface leads to the following expressions for r_e and p_e

$$\frac{r_e}{r_i} = \left[\frac{2(p_0 + s)}{(k+1)(p_i + s)}\right]^{1/(k-1)} \tag{38}$$

$$p_e = \frac{2p_0 - \sigma_c}{k+1} \tag{39}$$

3.3.2 Deformation Theory Constitutive Relations for Axisymmetry

The stress–strain relations in the yield zone, equations (13a–c) with $\lambda_x = \lambda_y = \lambda$, become

$$\varepsilon_r = \frac{1+\nu}{E_s}[(1-\nu)(\sigma_r - \lambda p_0) - \nu(\sigma_\theta - \lambda p_0)] \tag{40a}$$

$$\varepsilon_\theta = \frac{1+\nu}{E_s}[(1-\nu)(\sigma_\theta - \lambda p_0) - \nu(\sigma_r - \lambda p_0)] \tag{40b}$$

$$\varepsilon_{r\theta} = \sigma_{r\theta} = 0 \tag{40c}$$

and

$$\lambda p_0 = (E_s/E)p_0 + (1 - E_s/E)(\sigma_r + \sigma_\theta)/2 - E_s D(\gamma^p)/[2(1+\nu)(1-2\nu)] \tag{41}$$

The conventional flow rule of geomechanics used in conjunction with a Mohr–Coulomb failure criterion is recovered when

$$D(\gamma^p) = -\sin\phi^* \gamma^p \tag{42}$$

so that

$$\varepsilon^p_{kk} = -\sin\phi^* \gamma^p \tag{43}$$

or

$$k^* \varepsilon^p_1 + \varepsilon^p_3 = 0 \tag{44}$$

where ϕ^* is the (constant) dilatancy angle and $k^* = (1 + \sin\phi^*)/(1 - \sin\phi^*)$. (Note that $\phi^* = \phi$ implies an associated flow rule or normality.) Substituting the expression for γ^p from equation (18) in equation (42) implies

$$D(\gamma^p) = -2(1 + \nu)(1/E_s - 1/E)\sin\phi^*\tau \tag{45}$$

and equation (41) becomes

$$\lambda p_0 = (E_s/E)p_0 + (1 - E_s/E)(\sigma_r + \sigma_\theta)/2 + (1 - E_s/E)[\sin\phi^*/(1 - 2\nu)](\sigma_\theta - \sigma_r)/2 \tag{46}$$

3.3.3 Analytical Solutions for Displacements

3.3.3.1 No strain-softening

For completeness the solution for the displacements resulting from the excavation unloading problem when there is no strain-softening is recorded here

$$\frac{E}{1 + \nu}\frac{u}{r} = -\frac{(1 - 2\nu) + \sin\phi\sin\phi^*}{1 - \sin\phi\sin\phi^*}(p_i + s)\left[\left(\frac{r}{r_i}\right)^{k-1} - \left(\frac{r_e}{r_i}\right)^{k-1}\left(\frac{r_e}{r}\right)^{k^*-1}\right]$$
$$-(p_0 + s)\left[\frac{2(k - \nu(k + 1))}{k + 1}\left(\frac{r_e}{r}\right)^{k^*+1} - (1 - 2\nu)\right] \tag{47}$$

where, for simplicity, the expressions $\sin\phi$ and $\sin\phi^*$ as well as k and k^* have been used (see equations 20 and 44). This is similar to solutions to be found in the literature, *e.g.* Florence and Schwer [19], where the solution is for $k^* = k$ and for outer boundary loading.

Corresponding to the above displacements the expression for the total plastic strain (equation 16) is

$$\frac{E}{1 + \nu}\gamma^p = \frac{4(1 - \nu)\sin\phi(p_0 + s)}{1 - \sin\phi\sin\phi^*}\left[\left(\frac{r_e}{r}\right)^{k^*+1} - \left(\frac{r}{r_e}\right)^{k-1}\right] \tag{48}$$

and for the secant modulus

$$\frac{E_s}{E} = \frac{1 - \sin\phi\sin\phi^*}{2(1 - \nu)\left(\frac{r_e}{r}\right)^{k+k^*} - \sin\phi\sin\phi^* - (1 - 2\nu)} \tag{49}$$

For a dilatancy angle of zero, the expressions become

$$\frac{E_s}{E} = \frac{1}{2(1 - \nu)\left(\frac{r_e}{r}\right)^{k+1} - (1 - 2\nu)} \tag{50}$$

$$\frac{E}{1 + \nu}\gamma^p = 4(1 - \nu)\sin\phi(p_0 + s)\left[\left(\frac{r_e}{r}\right)^2 - \left(\frac{r}{r_e}\right)^{k-1}\right] \tag{51}$$

Clearly, equations (48) and (49) allow γ^p to be expressed in terms of $\frac{E_s}{E}$. Similarly, equations (50) and (51) lead to

$$\frac{E}{1 + \nu}\gamma^p = 2\sin\phi(p_0 + s)\left(\frac{2(1 - \nu)}{1 + (1 - 2\nu)\frac{E_s}{E}}\right)^{(k-1)/(k+1)}\frac{\left(1 - \frac{E_s}{E}\right)}{\left(\frac{E_s}{E}\right)^{2/(k+1)}} \tag{52}$$

This equation is not easy to invert, but shows that the strain-softening equation originally postulated (equation 23) is quite consistent with the more conventional expressions where postfailure cohesion varies with total plastic strain, γ^p.

Equations (47)–(51) were derived by Craig [20].

3.3.3.2 *Simplest approximation for strain-softening*

Prior to the development of the deformation theory formulation presented above, Duncan Fama [18] presented an analytical solution for the strains, displacements and also the modulus distribution E_s as a function of r. This model is equivalent to equations (40a–c) with a simplified λ.

The stress–strain relations were

$$\varepsilon_r = \frac{1+\nu}{E_s(r)}[(1-\nu+\beta)\sigma_r - (\beta+\nu)\sigma_\theta] \tag{53a}$$

$$\varepsilon_\theta = \frac{1+\nu}{E_s(r)}[(1-\nu-\beta)\sigma_\theta + (\beta-\nu)\sigma_r] \tag{53b}$$

with a constant dilatancy parameter β defined by

$$\varepsilon^p_{kk} = -(4\beta/E_s)\tau \tag{54}$$

With $E_s(r)$ replaced by a constant E, these relations were proposed by Pender *et al.* [21] to model prefailure dilatancy. This relation is recovered from equation (45) by neglecting E_s/E compared with 1, and setting β proportional to $\sin\phi^*$. All other contributions to λ are ignored, so that the pseudo *in situ* stress arises only from this simplified dilatancy term.

The simplest form of strain-softening was adopted with a constant reduced unconfined compressive strength $\sigma^*_c = \sigma'_c$ but no change in angle of internal friction in the yield zone. Then the stresses in the yield zone are given by equations (36a–c) with s replaced by

$$s' = \frac{\sigma'_c}{k-1} \tag{55}$$

The solution for the displacements as well as the modulus distribution was obtained in closed form

$$\frac{u}{r} = -\frac{1+\nu}{E}(p_0 - p_e)\left[\frac{\left(\frac{r}{r_i}\right)^{k-1} - h}{\left(\frac{r_e}{r_i}\right)^{k-1} - h}\right]^{\frac{b-1}{k-1}} \tag{56}$$

with

$$E_s(r)\frac{u}{r} = -(1+\nu)(1-2\nu)\left[\left(\frac{r}{r_i}\right)^{k-1} - h\right]s'/h \tag{57}$$

with the parameters b and h given by

$$b = \frac{1-\nu+\beta-(\nu+\beta)k}{(1-\nu-\beta)k+\beta-\nu} \tag{58a}$$

$$h = \frac{(1-2\nu)s'}{[(1-\nu-\beta)k+\beta-\nu](p_i+s')} \tag{58b}$$

An analytical solution was also obtained for the nonlinear Hoek–Brown failure criterion on the stresses.

3.3.3.3 *Analytical solution for a smooth cohesion reduction in the yield zone*

We replace the discontinuous drop of unconfined compressive strength from σ_c (prefailure) to σ^*_c in the yield zone by a continuous reduction as follows.

Postulating a dependence on minor principal stress or confinement, suppose that we replace equation (23) with

$$\sigma^*_c = \chi\sigma_3 + \sigma'_c \tag{59}$$

for some χ chosen so that $\sigma_c^*(r_e) = \sigma_c$. Here σ'_c is the limiting value of unconfined compressive strength for zero confinement. This implies that

$$\chi = \frac{\sigma_c - \sigma'_c}{p_e} \tag{60}$$

Thus the postfailure yield criterion, instead of equation (22), becomes

$$\sigma_\theta = (k + \chi)\sigma_r + \sigma'_c \tag{61}$$

so that in the yield zone we have an apparently higher friction angle, but a smaller cohesion. Note that p_e (equation 39) and hence χ depend on p_0 as well as σ_c and ϕ, and this is less suitable than a strain measure. In fact the pre- and post-failure curves are bilinear, meeting at the point represented by the yield–elastic interface for the problem. In Figure 1 the continuous line shows the prefailure and the dashed line the postfailure criteria relevant to the parameters of problem 2 of Section 3.4.

It is clear that the solutions already derived in Sections 3.3.1 and 3.3.3.2 are immediately applicable to this postfailure curve. In fact the solution for a prefailure yield criterion given by equation (33) together with a postfailure yield criterion given by equation (61) is identical to that for both pre- and post-failure yield criteria given by equation (61). (The continuation of the postfailure line is shown as a dotted line in Figure 1.) $k + \chi$ replaces k and σ'_c replaces σ_c everywhere in the expressions for the solution. (It is easy to verify, for instance, that replacing σ_c by σ'_c and k by $k + \chi$ in equation 39 for p_e leaves the expression unchanged, and also that no stress points in the elastic region ($\sigma_3 > p_e$) lie between the continuous and the dotted lines in Figure 1).

This means that the solution for the displacements in equation (47) is valid and thus an analytical solution is available for a strain-softening problem (with an arbitrary dilatancy angle).

It is interesting to examine the somewhat unconventional strain-softening equation (59) and determine the variation of unconfined compressive strength with total plastic strain. The results of this model can then be compared with results obtained when the strain-softening is controlled by this variation (*e.g.* FLAC [23] or FESOFT [22], which has both options). Section 3.4 describes these codes in detail. For simplicity, using the case where there is zero dilatancy, replacing k by $k + \chi$ as well as σ_c by σ'_c, we note first that equations (36a–c) with equation (38) implies that

$$\sigma_r = \frac{2(p_0 + s')}{k + \chi + 1}\left(\frac{r}{r_e}\right)^{k+\chi-1} - s' \tag{62}$$

where

$$s' = \frac{\sigma'_c}{k + \chi - 1} \tag{63}$$

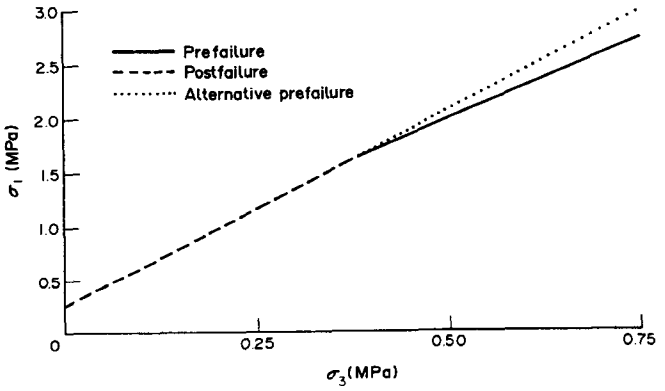

Figure 1 Approximate pre- and post-failure yield criteria

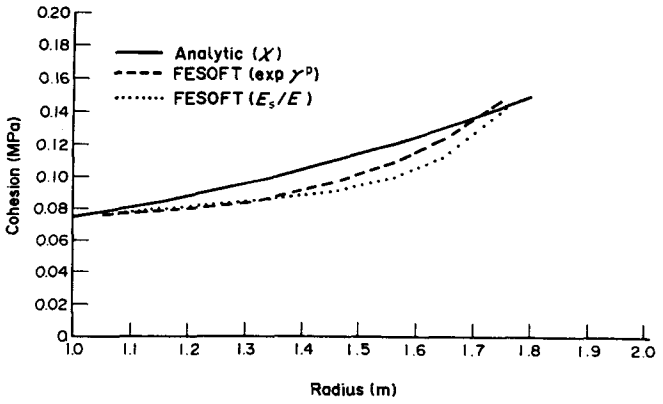

Figure 2 Cohesion across yield zone

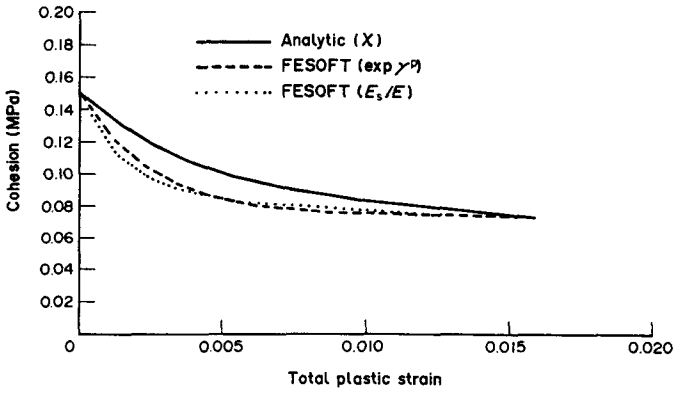

Figure 3 Cohesion against total plastic strain

Substituting for (r/r_c) in equation (51) gives the following relationship between γ_p and σ_r

$$\frac{E}{1+\nu}\gamma^p = (1-\nu)(k+\chi-1)(\sigma_r+s')\left[\left(\frac{(k+\chi+1)(\sigma_r+s')}{2(p_0+s')}\right)^{-\frac{k+\chi+1}{k+\chi-1}} - 1\right] \tag{64}$$

We could substitute for $\sigma_r = \sigma_3$ from equation (59), which gives γ^p in terms of σ_c^*. This is not readily invertable to yield a closed form expression for σ_c^* in terms of γ^p. However, it is not difficult to solve equation (64) and equation (59) numerically. Figure 2 shows the variation of cohesion across the yield zone and Figure 3 shows the variation with total plastic strain. These are for the parameters of problem 2 (see Table 4) below.

The continuous curve (labeled Analytic χ) is obtained by using equation (59) and the dotted curve (labeled FESOFT E_s/E) is obtained by using equation (23) with $\alpha = 1$. For comparison purposes, the dashed curve (labeled FESOFT $\exp\gamma^p$) is obtained with a more conventional strain-softening relation

$$\sigma_c^* = \sigma_c - (1 - \exp^{-\gamma_p/\delta})(\sigma_c - \sigma_c') \tag{65}$$

with $\delta = 1/400$. The latter two give nearly identical results – the analytical solution is clearly a useful alternative, without the flexibility of either equation (23) or of equation (65), where α or δ can be varied to give a fast or a slow decay of σ_c^* from its initial to its final value. In fact for $\delta = 1/200$ the analytical solution is nearly identical to the numerical solution obtained using equation (65).

Note that equation (64) which relates γ^p and σ_r also yields an analytical relationship between shear strain and shear stress. The form of the shear stress *versus* shear strain curves resulting from the strain-softening assumptions of each model is shown in Figure 4.

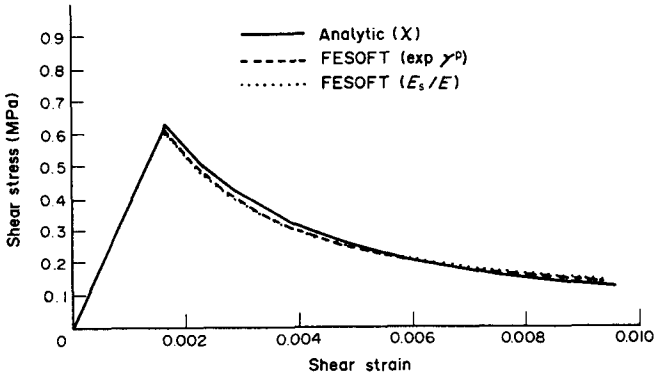

Figure 4 Shear stress against shear strain

There are obvious difficulties in extending equation (61) to nonaxisymmetric problems, because it is not clear what value to take for p_e in equation (60). However, equations (59) and (60), with a suitable estimate of p_e, were used successfully in a study of coal mine chain pillar stability (Duncan Fama and Wardle [17]).

3.3.3.4 Approximation for λ in deformation theory

The displacements and strains given in Section 3.3.3.1 are relatively complicated, but a good approximation for λ can be used to obtain a very simple analytical solution. Replacing equation (41) by

$$\lambda p_0 = (\sigma_r + \sigma_\theta)/2 \tag{66}$$

can be expected to give a reasonable approximation. For, referring to equation (46), we note that for the two limiting cases: (i) $E_s \approx E$, (*i.e.* near the yield–elastic zone interface) $\lambda \approx 1$ as we would expect. Since $(\sigma_r + \sigma_\theta)/2 = p_0$ in the elastic region, $(\sigma_r + \sigma_\theta)/(2p_0) \approx 1$ also; and (ii) $E_s \ll E$ (*i.e.* near the opening), λ is of the order of $(\sigma_r + \sigma_\theta)/(2p_0)$ provided E_s/E is of this order or smaller.

This approximation is useful because it allows a very simple analytical solution to be obtained with a nonzero pseudo *in situ* stress field.

An interesting feature of this choice of λ is that λp_0 is exactly that level of *in situ* hydrostatic stress at which the elastic stresses at the point r lie on the yield surface. For, in that case

$$\sigma_r = \lambda p_0(1 - A/r^2) = (p_i + s')\left(\frac{r}{r_i}\right)^{k+\chi-1} - s' \tag{67a}$$

$$\sigma_\theta = \lambda p_0(1 + A/r^2) = (k + \chi)(p_i + s')\left(\frac{r}{r_i}\right)^{k+\chi-1} - s' \tag{67b}$$

$$\sigma_{r\theta} = 0 \tag{67c}$$

for some constant A, and these equations express the fact that the stresses at the point r satisfy the yield criterion and also the elastic solution for an *in situ* stress in the far-field of λp_0.

In the incremental theory of plasticity, the loading would be applied in increments until precisely this level is reached. Further increments of load are, in fact, 'removed' and must be carried by neighboring elements.

Note that in the incremental plasticity theories the element would continue to strain in this process – in the technique described here this is also true to the extent that as more elements fail the modulus of each element drops further to keep the stresses on the yield surface. This is done iteratively not incrementally. The process has been described in detail in Section 3.2.5.

The stress–strain relations in the yield zone simplify to

$$\varepsilon_r = -\frac{1+\nu}{2E_s}[\sigma_\theta - \sigma_r] \tag{68a}$$

$$\varepsilon_\theta = +\frac{1+\nu}{2E_s}[\sigma_\theta - \sigma_r] \tag{68b}$$

$$\varepsilon_{r\theta} = \sigma_{r\theta} = 0 \tag{68c}$$

Since the right hand sides of these equations are proportional to the components of s_{ij} in polar coordinates, equations (68a–c) are just equation (3) with E^* replaced by E_s and ε^p_{ij} replaced by ε_{ij}. Thus this choice of λ is equivalent to neglecting the elastic strains ε^e_r and ε^e_θ in the yield zone in comparison to the plastic strains and also setting

$$\varepsilon^p_{kk} = D(\gamma^p) = 0 \tag{69}$$

Equations (68a–c) (with E_s replaced by E) are also valid in the elastic zone (refer to equations (40a–c)) with $E_s = E$ and $\lambda = 1$ and replace p_0 by $(\sigma_r + \sigma_\theta)/2$). Thus

$$\varepsilon_r + \varepsilon_\theta = 0 \tag{70}$$

throughout the medium.

Since $\varepsilon_r = du/dr$ and $\varepsilon_\theta = u/r$ (where u is the displacement in the medium), equation (70) implies that $du/dr + u/r = 0$ with solution $u = C/r$ everywhere. Here C is a constant which is to be determined from the boundary and interface conditions.

u_e, the displacement at r_e, is obtained from equation (68b) (with $E_s = E$), using equations (35a–c) for the stresses in the elastic region. Thus

$$u = \frac{u_e r_e}{r} = -\frac{(1+\nu)}{E}\frac{(p_0 - p_e)r_e^2}{r} \tag{71}$$

(with p_e given by equation 39) where we have used the expressions for the stresses in the elastic zone together with the stress–strain relations to obtain u_e.

Although the form $u = C/r$ of the displacement solution is exactly the same as for the linear elastic solution, we note that the displacement at the opening surface $r = r_i$ is substantially greater as the yield zone width increases. With no yield and no support pressure at $r = r_i$, equation (71) with $p_e = 0$ and $r_e = r_i$ gives

$$u = -\frac{1+\nu}{E}\frac{p_0 r_i^2}{r} \tag{72}$$

When the parameters are those of example 2 of Brown *et al.* [15] and Duncan Fama [18], namely $r_i = 5.35$ m, $p_0 = 3.31$ MPa, $p_i = 0$, $E = 1.38$ GPa, $\nu = 0.25$, $k = 4$, $\sigma_c = 2.4$ MPa and $\sigma'_c = 0.024$ MPa, the computed values of u_e and u_i (the displacement at r_i), for the two solutions are $u_e = 7$ mm and $u_i = 16$ mm for the elastic solution, and $u_e = 30$ mm and $u_i = 75$ mm for the elastic plastic solution. Here σ'_c was chosen to match the yield zone width to that of Brown *et al.* [15] with postfailure defined by equation (61). The value of u_i computed for the elastic plastic solution for this model is virtually identical to that computed numerically by Brown *et al.* with a small value for their dilatancy parameter.

3.4 PLANE STRAIN PROBLEMS FOR CIRCULAR EXCAVATIONS

We consider first a circular excavation under an *in situ* stress $\sigma^0_x = p_0 + S_0$ and $\sigma^0_y = p_0 - S_0$ and $\sigma^0_{xy} = 0$ which is not hydrostatic. Detournay [13] defined an obliquity

$$m = S_0 \Big/ \left[\frac{k-1}{k+1}\left(p_0 + \frac{\sigma_c}{k-1}\right)\right] \tag{73}$$

and studied problems for which $m \leq 0.3$. Here the yield zone completely surrounds the excavation and the stresses in the yield zone are statically determined and identical to those in the axisymmetric

case. The deformation theory is again valid and the numerical results are identical to Detournay's analytical results [13].

A series of comparison runs were done on circular excavation problems with the two-dimensional finite element code FESOFT [22] using the deformation theory of plasticity described above and with the two-dimensional finite difference code, FLAC [23], which uses the incremental theory of plasticity and allows strain-softening. The results are tabled below together with results from Detournay's program KINEDI [13] which also uses incremental theory.

A circular excavation with radius 1 m was analyzed. The radial nodes for both the finite element (FESOFT) and the finite difference mesh (FLAC) were at 0.1 m intervals from 1 m to 3 m, at 0.25 m intervals to 5 m, then 1 m intervals to 8 m, then 2 m (2), 3 m and 5 m (3) intervals to the outer boundary of 30 m (38 nodes on each spoke). The quadrant $x > 0$, $y > 0$ was divided into 20 equal spokes (see Figure 6).

Two problems were analyzed, one ideal plastic and one with strain-softening. The parameters were chosen so that both had a yield zone width of approximately one radius for axisymmetric *in situ* stresses. It can be seen from the results that the solutions are very similar in both cases.

The following parameters were common to both problems: $p_0 = 1$ MPa; $p_i = 0$; $E = 1$ GPa; $\nu = 0.3$; $k = 3.0$; and $k^* = 2.0$. For problem 1 (ideal plastic) the cohesion, c, and postfailure cohesion c^* were given by $c = c^* = 0.092$, so that $\sigma_c = \sigma_c^* = 0.32$.

Table 1 compares displacements at the x and y axis excavation boundary for problem 1, for the three programs for $m = 0$ (axisymmetric) and $m = 0.3$. FESOFT and FLAC results only are compared for the ratios of *in situ* stress $\sigma_x^0/\sigma_y^0 = 0.5$ and 0.4, where $(\sigma_x^0 + \sigma_y^0)/2 = p_0 = 1$ MPa.

For problem 2, $c = 0.15$ MPa and $c' = 0.075$ MPa. The strain-softening relation used in FESOFT is as given in equation (23) with $\alpha = 1$, and the relation used for FLAC was fitted to the scatter plot obtained from the FESOFT results as shown in Figure 5. (Note that the FLAC γ^p is one-half of our γ^p.)

Table 2 compares displacements at the x and y axis excavation boundary for the strain-softening problems for the same four *in situ* stress ratios as above.

A more detailed comparison of the results of FESOFT and FLAC for the strain-softening case where $\sigma_x^0/\sigma_y^0 = 0.4$ is shown in Figures 6–10. The agreement is remarkable, particularly in view of the difference in the strain-softening models. The FLAC2 results agree better than FLAC1 which looks like a better fit to the scatter plot. However, the slower decay in FESOFT to the final cohesion values is important and the results show that the γ^p values for FLAC2 are more comparable with the FESOFT values, particularly in the region of greatest yield.

Figure 6 shows the deformed mesh and the yield zones resulting from the two analyses. The intensity of yield is measured in FLAC by the total plastic strain, whereas in FESOFT it is reflected in the ratio of the secant modulus E_s (equations 13a–c) to the modulus, E, of the intact material. The few edge elements that yielded in the FLAC analysis but not in the FESOFT analysis are shown. The total plastic strain in these elements was in all cases less than 1% of its value near the opening boundary on the x axis. The ranges of E_s/E are shown in the legend to the figure. In fact, half the elements in the inner ring had a secant modulus E_s which was only 1% of E. The modulus reduction for the ideal plasticity analysis was similar.

Figure 7 shows the displacements around one quadrant of the opening boundary, and Figure 8 shows the corresponding major and minor stresses there.

Figures 9 and 10 show the major and minor stresses on the x and y axes from the far-field (at radius 30 m) at left to the opening boundary (radius 1 m) at right, respectively.

The number of iterations for FESOFT is normally taken so that the minimum value of F_{os} (see equation 32) in any element is at least 0.99. For the size of yield zone in the ideal plasticity problems above this required about 25 iterations. The strain-softening problems required 35. The minimum F_{os} was 0.999 when the iterations were increased to 42 (ideal plasticity) or 60 (strain-softening). The

Table 1 Normal Displacements (mm) at Excavation Boundary on the Axes for Problem 1

σ_x^0/σ_y^0	m	*KINEDI*		*FLAC*		*FESOFT*	
		x axis	*y axis*	*x axis*	*y axis*	*x axis*	*y axis*
1.0	0.0	5.4	5.4	5.3	5.3	5.3	5.3
0.705	0.3	7.6	3.9	7.5	4.6	7.5	4.0
0.5	0.57			10.5	5.5	10.2	4.1
0.4	0.74			13.2	6.4	12.8	4.8

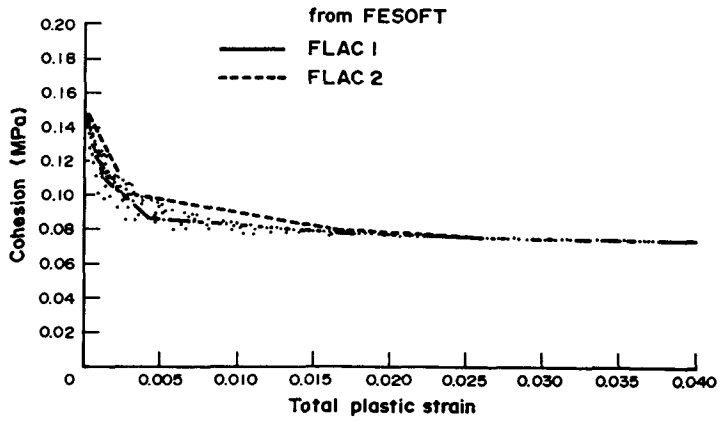

Figure 5 Total plastic strain, γ^p

Table 2 Normal Displacements (mm) at Excavation Boundary on the Axes for Problem 2

σ_x^0	σ_y^0	*FLAC1*		*FLAC2*		*FESOFT*	
		x axis	*y axis*	*x axis*	*y axis*	*x axis*	*y axis*
1.0	1.0	5.5	5.5	4.8	4.8	5.7	5.7
0.83	1.17	7.0	3.4	7.8	3.2	8.4	3.7
1.33	0.67	12.9	4.2	11.9	4.0	11.4	3.9
1.43	0.57	16.0	5.7	14.9	4.8	14.3	4.6

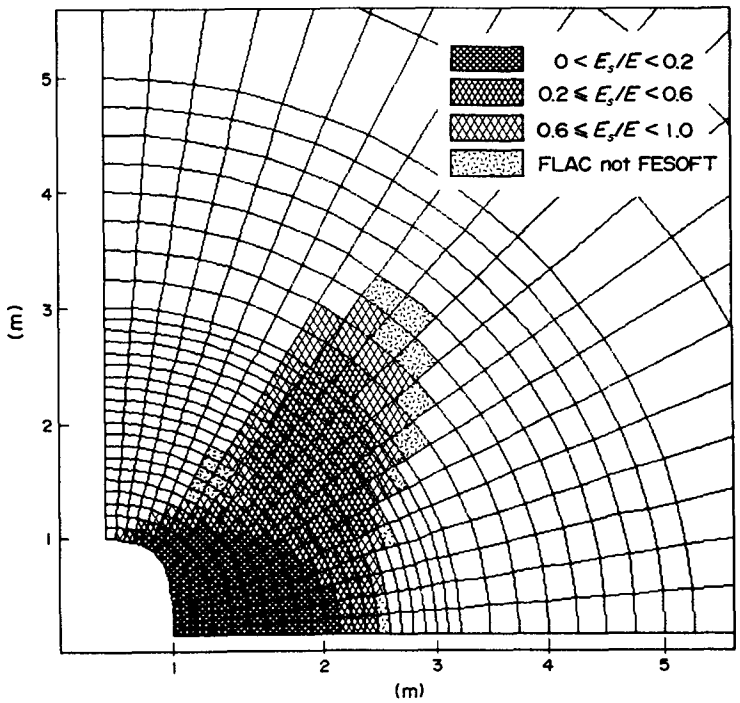

Figure 6 Yield zone for $\sigma_x^0/\sigma_y^0 = 0.4$ with strain-softening

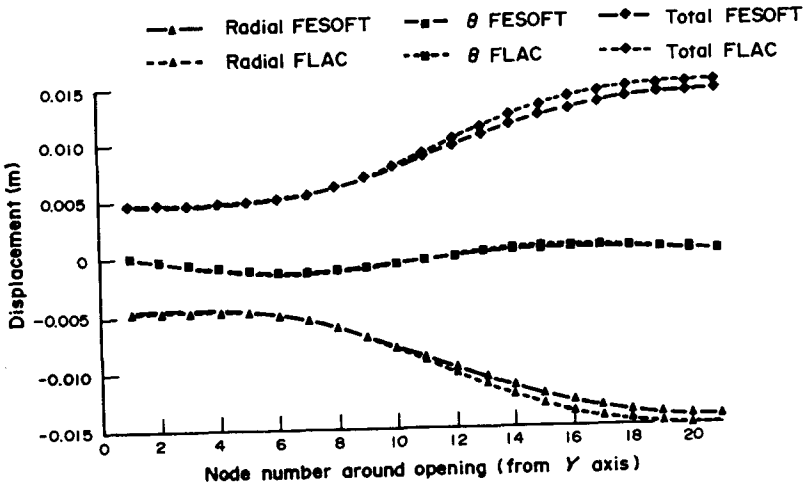

Figure 7 Displacements on opening boundary quadrant

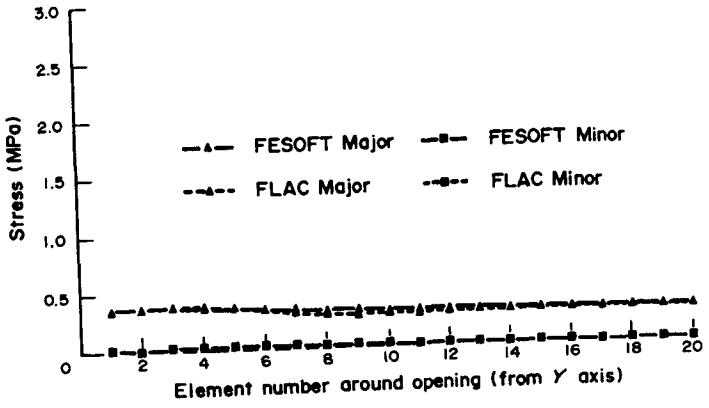

Figure 8 Major and minor stresses around opening boundary quadrant

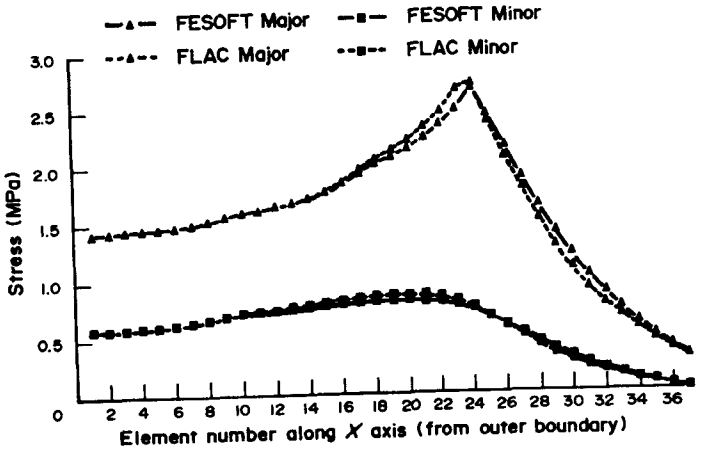

Figure 9 Major and minor stresses along x axis

cpu time also depends on the size of the yield zone. It is not possible, at present, to compare run times of FESOFT and FLAC on the same hardware. The cpu time for the FESOFT strain-softening run (with 60 iterations) on a SUN 3/110 workstation was 1 h, and on a CONVEX 120 was 150 s.

It is important to note that, for a coarse mesh, the iterative procedure will underestimate the yield zone width, the modulus reduction and hence the opening displacement. For problem 1 above,

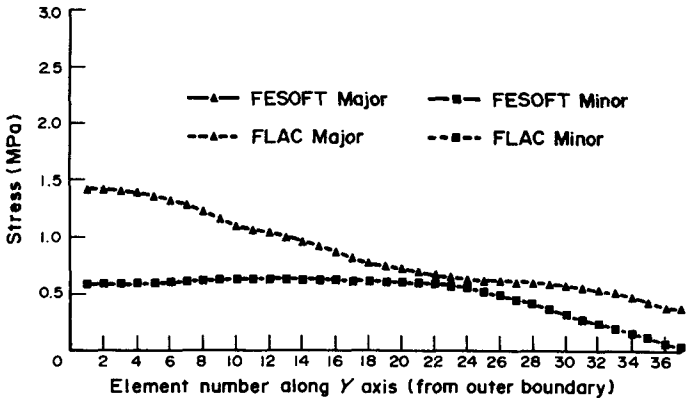

Figure 10 Major and minor stresses along *y* axis

Table 3 Opening Displacement and Average Moduli for Three Different Meshes

Mesh	*Displacement*	*Average modulus (inner)*	*Average modulus (outer)*
1	0.33	127	449
2	0.31	137	491
3	0.26	185	730

Table 3 shows the results for the axisymmetric solution with $k^* = 1$ for three different meshes. Mesh 1 is the mesh shown in Figure 6 and has the yield zone divided into nine rings. Mesh 2 and mesh 3 have respectively four and two rings in the yield zone. The displacement tabled is at the opening, and the modulus is averaged over the two rings which constitute the yield zone for mesh 3. Note that a one-ring mesh cannot be used as the elastic stress at the midpoint does not violate the yield criterion.

The results in this section confirm the validity of the use of deformation theory for circular excavations with the Mohr–Coulomb yield criterion, even with some strain-softening.

3.5 APPLICATION TO UNDERGROUND COAL MINING IN AUSTRALIA

FESOFT has been used to model deformation and yield around coal mine roadways in Australia. Much of the underground coal mining in this country is done in coal seams about 3 m thick sandwiched between sandstone interspersed with mudstone. Thus the roof and floor of the roadways are stiff and strong in comparison with the coal. Typically, the horizontal *in situ* stress in the roof and floor strata in one direction is twice as high as the vertical, whereas the horizontal stress in the other direction is of the order of the vertical. The *in situ* stresses in the coal seams are believed to be closer drostatic. Figure 11 shows a simplified core log and the roadway geometry to be modeled.

hus conditions encountered in drivage of roadways are very dependent on the direction in relation to the major principal stress [24]. When a roadway is driven at an angle greater than about 30° to the major principal stress, shear fracturing on one side of the roof and floor can occur, requiring expensive remedial measures in the way of extra support.

It has been found that one substantial benefit accrues from the presence of the fractured region around the roadway. A neighboring road can be driven in the stress shielded region nearby and this road experiences no adverse roof or floor behavior. It has become clear that the most important mechanism dictating the protection of the second road is the reduction in horizontal stress in the roof and floor because of the shear fractures around the first road. The protected road can be driven 40 m away from the first, depending on the severity of the fractures [25].

order to model this situation FESOFT was enhanced to allow excavation sequencing. In addition a simple joint element similar to that described by Beer [26] was implemented. This was to

pare run times
-softening run
was 150 s.
ir-ate the yield
1 above,

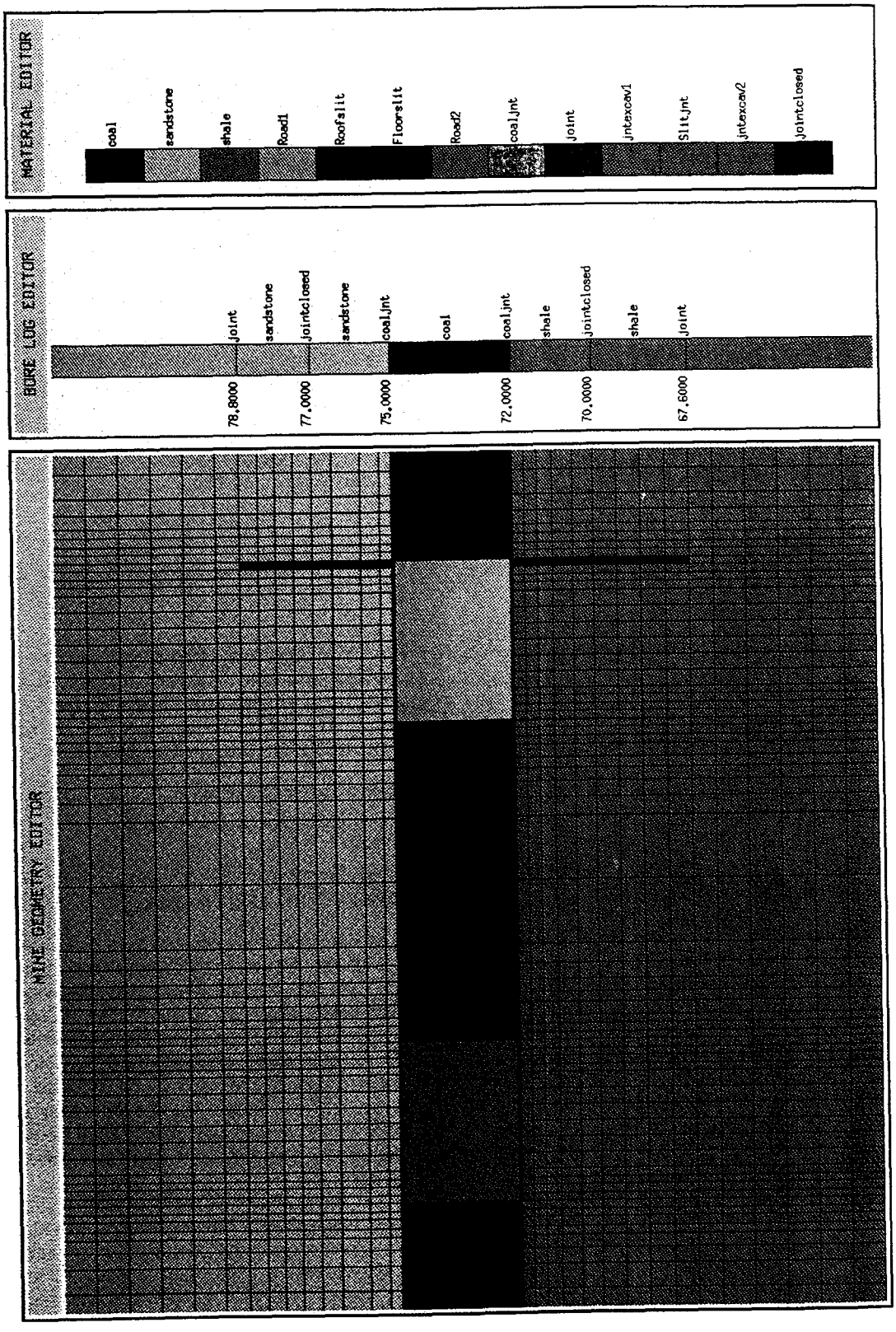

Figure 11 Geol[illegible]l core log and roadway ge[illegible] to be modeled

Material
Roof
Coal
Floor

cater fo
strengt
from th
Two
assume
normal
weaker
from th
The
540 m
one is
The h
bound
layers
assum
vertica
The
norma
deform
A fi
spite
reduc
subst
reduc
yield
colore
Thi
princi
driver
roadw
impo
are h
allow
tions
width
the s
plane
roof
fract
fract
geom
pres
this
suffe
the
whe
T
diffe
or th
join

Table 4 Geomechanical Parameters and *in situ* Stresses for Coal Mine Roadway Analysis

Material	E (GPa)	ν	σ_c (MPa)	k	σ_c^*	k^*	σ_y (MPa)	σ_x (MPa)
Roof	3300	0.3	17.0	3.7	5.7	2.0	15	30
Coal	850	0.3	5.1	3.7	1.7	2.0	15	12.5
Floor	2000	0.3	11.1	3.7	3.7	2.0	15	20.7

cater for observed movement along bedding planes in the roof and floor of the roadway. Low shear strength on these bedding planes also contributes to the lack of build-up of horizontal stress away from the fracture.

Two roadways of dimensions 6 m wide and 3 m high are driven, separated by a 12 m pillar. It is assumed that they are driven at an angle greater than 30° to the major stress. The roads will normally be supported with rock bolts, but the effect of these is well modeled by less postfailure weakening of the strata than would occur otherwise. The roof has bedding planes 1.6 m and 4 m from the coal seam, and the floor has bedding planes 1.8 m and 4.5 m from the seam.

The *in situ* stresses are taken to be 15 MPa vertical (corresponding to a depth of cover of about 540 m), and 30 MPa horizontal in the stiff roof. (A horizontal to vertical *in situ* stress ratio of two to one is commonly measured in the roof strata above seams in the Sydney Basin of New South Wales.) The horizontal stress in the other layers varies with the stiffness in such a way that, if the outer boundaries of the mesh were to be loaded, constant strains everywhere and uniform stresses within layers would result. This leads to nearly hydrostatic conditions in the coal seam. The parameters assumed for the different layers are given in Table 4, with the resulting horizontal (and assumed vertical) *in situ* stress in the final columns.

The joints were all given a prefailure cohesion of 1 MPa and an angle of friction of 30°. Postfailure normal and shear stiffnesses are reduced in a similar way to the modulus of elasticity for the deformation theory until the stresses satisfy the yield criterion.

A first attempt at modeling this situation failed to show much protection of an adjacent road in spite of extensive yield around the first driven road. The failure properties of the roof and floor were reduced quite substantially (σ_c to 25% of values above, with $k = 3$) but the model still predicted substantial yield in the roof and floor of the second roadway. The horizontal stress is very much reduced in the yield zone around the road but returns quite rapidly to its *in situ* level away from the yield zone. The two roads are shown in Figure 12. The first road driven is on the right. The deeper colored regions are the yield zones, the modulus factor denoting E_s/E.

Three-dimensional analysis of a single roadway driven in an unfavorable direction to the major principal stress [24] predicts a stress concentration on one side of the roof and floor of the first driven road. This is confirmed by *in situ* observations of a massive shear fracture on one side for such roadways. This shear fracture is typically at a low angle to the vertical (10° or 20°). Clearly it is impossible to model this with a two-dimensional vertical slice through the roadway, when the strata are homogeneous. It was decided to model the sequence of events by introducing the first roadway, allowing yield and deformation in the same way as has been described above for circular excavations, and then, in increment two, which is a new deformation theory analysis, a vertical slit of finite width (300 mm) and height 4 m (4.5 m) in the right hand side of the roof (floor) is removed, to model the shear fracture. The respective heights are so that the slit extends to the upper (or lower) bedding plane. The slit thus operates as a separated joint of finite width – the width is necessary so that the roof (floor) plate can move towards the fracture. What has been observed *in situ* is that the roof fractures up to a parting plane, which then separates. As the roof plate sags away from the inclined fracture, it also slips along the parting plane. Modeling this exactly requires a program with geometric nonlinearity, but the stress shielding mechanism is modeled nearly perfectly by the presence of the slit. A third increment excavates the second road. Figure 13 shows the final result for this analysis. It shows clearly that the roof of the second road does not yield at all and the floor suffers only very mild yield. The coal ribs do yield, however. Also well modeled is the movement of the roof and floor along the bedding planes towards the fracture. The floor slit is just about closed, whereas the roof slit is about one-third of its original width.

The artificial introduction of the slit to model the fracture is perhaps open to criticism, but is no different in principle from the choice of block sizes and orientations in the discrete element method or the placement of weak joints in preferred positions. What is interesting here is that a low strength joint will not have the desired effect unless separation occurs because the horizontal stress will be

Figure 11 Geological core log and roadway geometry to be modeled

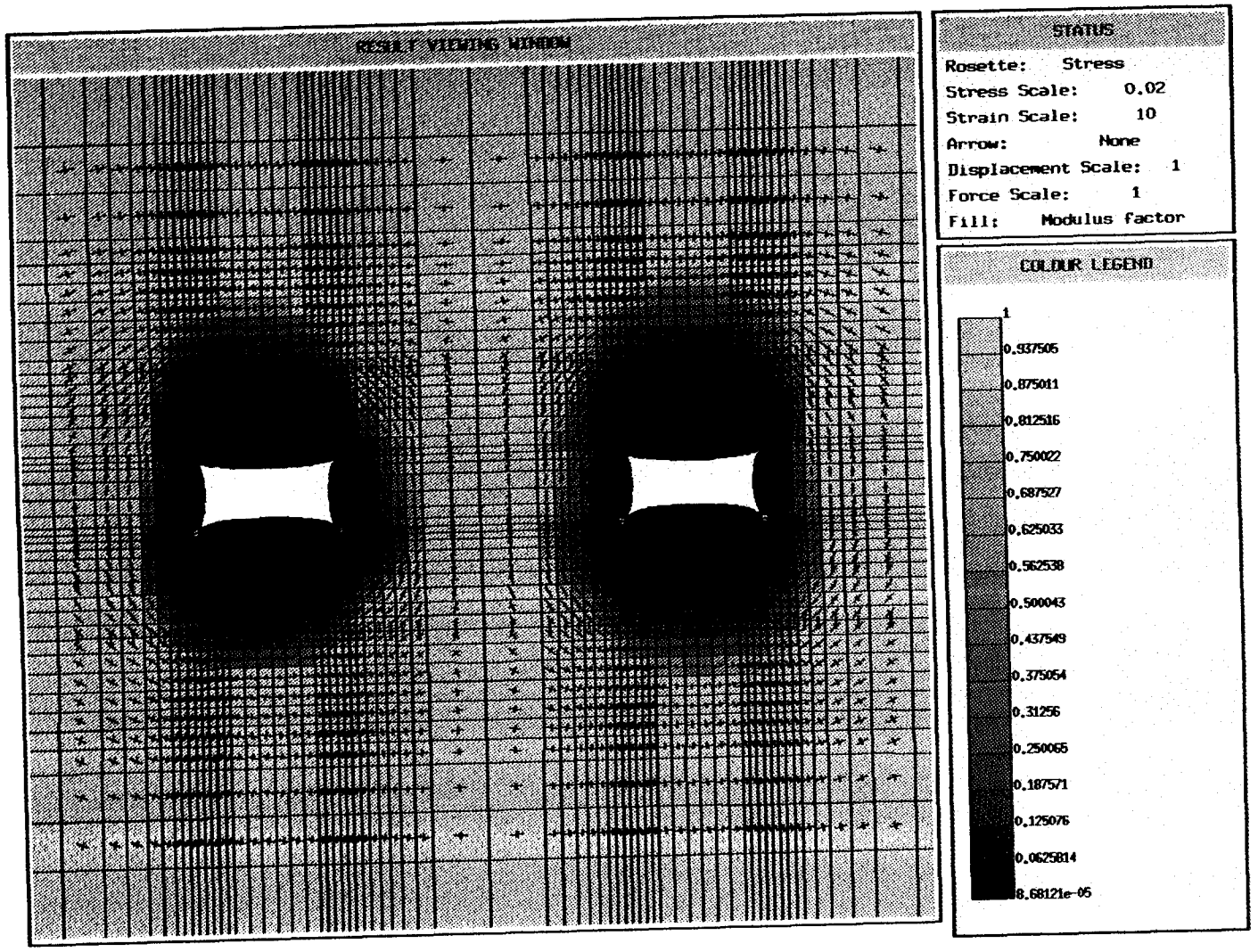

Figure 12 Two roads with yielded and softened roof and floor

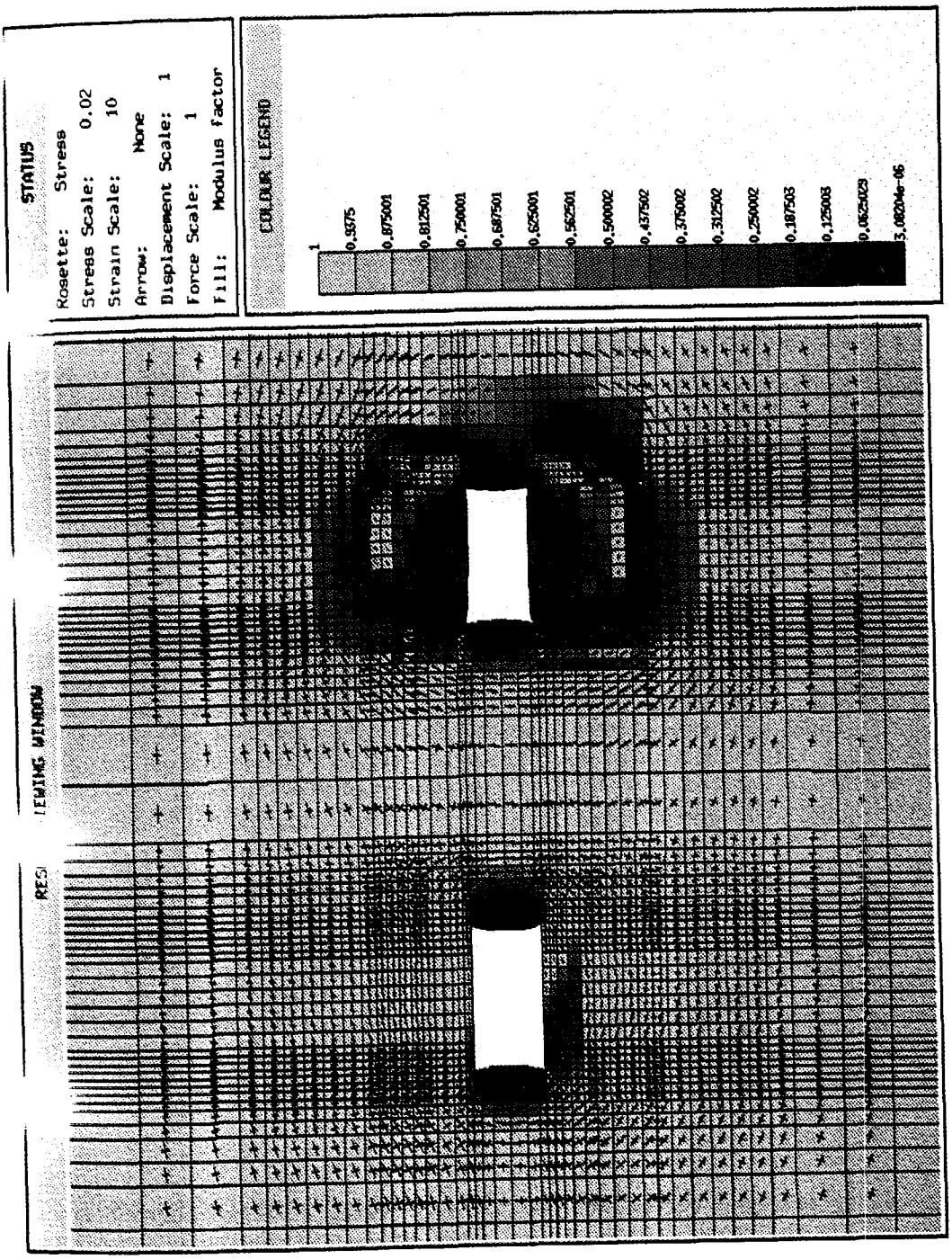

Figure 12 Two roads with yielded and softened roof and floor

Figure 13 Two roads with slit in roof and floor of right road

transmitted across the joint if it only fails in shear. Also shear movement along the bedding planes will only occur if both the fracture joint and the bedding plane where it intersects this joint fail in tension and separate. Research is ongoing with this and other models to improve our ability to model real *in situ* observations. The detailed and careful modeling of onset and development failure (*e.g.* [27] and [28]) will eventually be incorporated into numerical codes and will be able to be used to model this sort of situation. The other major challenge is the determination of realistic input parameters to the models.

3.6 THE IMPORTANCE OF THE PSEUDO *IN SITU* STRESS

Clearly the parameter λ which controls the level of pseudo *in situ* stress is a key element of the numerical calculation procedure. It is becoming a common procedure to model a supposedly yielded region [6, 7] or caved waste [1] by a material of lower modulus of elasticity. Naturally, for excavation unloading problem, the *in situ* stress in the element is not reduced, which means that λ is taken as unity. The one exception (known to this author) to this is contained in a paper by Kaiser [29]. Kaiser points out that a nonlinear response of a circular opening to excavation and support may be described by the response of the same sized opening in linear elastic ground of different stiffness and under a reduced stress field. Later in the same paper, Kaiser states 'the observations made at the Kielder Tunnel indicate a softened (not necessarily weakened) zone of rock near the tunnel wall. This finding is significant because it is in strong disagreement with the generally accepted concept of a strain-weakening, plastic zone (Egger [30]) of overstressed rock near the tunnel.' We will demonstrate that the softened ring Kaiser used was actually an excellent approximation to a strain-weakening, plastic zone!

For simplicity, we will confine the discussion to an axisymmetric *in situ* stress and we will ignore dilatancy, so that $k^* = 1$. (However, dilatancy can be incorporated in the analysis without difficulty.) The displacement at the opening boundary obtained from FESOFT for the mesh described above with the parameters of problem 2 (see Section 3.4) but $k^* = 1$, is 3.3 mm (compare this with the FESOFT result in Table 2 of 5.7 mm for $k^* = 2$). Note that the stresses do not vary with k^*.

We will attempt to model the yield zone with one ring of the same width ($1 \leq r \leq 1.8$) of reduced modulus and reduced *in situ* stress, bonded to the intact linear elastic medium of infinite extent ($r \geq 1.8$). Using the analysis for a linear elastic ring bonded to a semiinfinite elastic medium of different modulus (see Appendix), the correct displacement is obtained when the modulus of elasticity of the softened inner ring is taken to be 0.184 GPa and $\lambda = 0.60$ (to satisfy equation 76 with $p_i = 0$). For these values, the curve labeled 'λ Correct' in Figure 14 shows that not only does the opening displacement agree with the FESOFT strain-softening analysis results, but the interface displacement (1.5 mm) also agrees exactly. In fact it can be seen from Figure 14 that the solution in the outer elastic ring is identical to the FESOFT results.

Referring to Figure 15, and again comparing the curve labeled 'λ Correct' with the FESOFT results, we see that the radial stress in the inner ring is moderately well modeled at the opening boundary, although it is about double the true value at the midpoint. The hoop stress is well approximated at the midpoint, and displays the usual opposite trend across the ring to the true solution. The relation between the midpoint stresses is not at all close to the original yield criterion.

What is of great practical importance is that the displacement is so well modeled everywhere. This means that if extensometer measurements in a pilot hole in an axisymmetric stress field are well modeled by this crude two-ring analysis, we can be reasonably confident that the medium is also well modeled by a Mohr–Coulomb criterion with strain-softening as in Section 3.3.3.3. It seems certain that the pre- and post-failure properties of the medium will be able to be inferred from the extensometer readings. This will be the subject of a future publication.

Stress measurements in the elastic region can also be compared with the predictions of the two-ring analysis. The fact that the stresses in the yield zone are not well described should be noted but is not a great practical disadvantage because stress measurements in a yielded region are not possible.

Figures 14 and 15 also show the results obtained from using $\lambda = 1$ and also the λ obtained from the approximate expression in equation (66) in the yield zone. In both cases the modulus reduction of the ring was chosen to obtain the correct opening displacement. The displacements at the interface of the yield zone and the elastic zone, in these two cases, are rather poorly approximated. In the $\lambda = 1$ case, the displacement is 75% of the true value, in the case of the approximate λ the displacement is 122% of the true value. This demonstrates clearly the importance of getting the pseudo *in situ* stress in the yield zone right (*i.e.* computed according to equation 46).

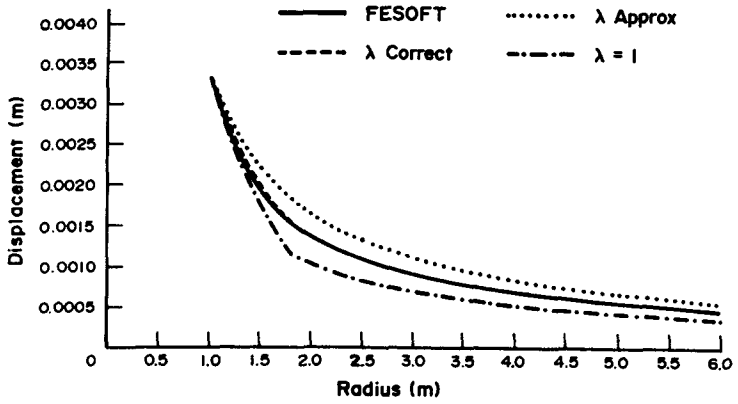

Figure 14 Displacement distributions for different λ models

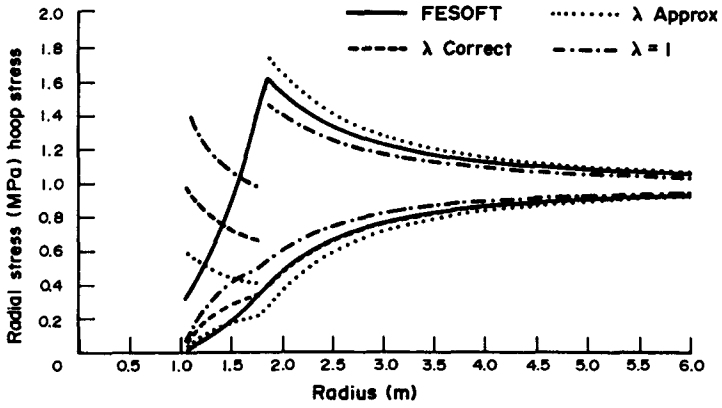

Figure 15 Stress distributions for different λ models

The analytical approximation in Section 3.3.3.4 gives the stress distribution perfectly. This shows that the expression for the reduction of unconfined compressive strength (equation 61) for the approximate solution is very close to that assumed in equation (23), at least for this problem. The displacements in the elastic region are correct, but the solution predicts only 80% of the opening displacement.

3.7 CONCLUSION

The work described here aims to model yield zones in weak rock in a relatively simple manner, and with a view to numerical computation. The widespread practice of modeling yield zones by a homogeneous material of lower stiffness than the intact material is shown to be, potentially, an excellent approximation to the deformation theory of plasticity. An important point has been emphasized – namely that the *in situ* stress unloaded from these regions of low stiffness must also be reduced.

We note that the theory and examples in this chapter have used the simpler Mohr–Coulomb yield criterion to limit the stresses around the excavation. The method can equally be applied to the Hoek-Brown or other nonlinear failure criteria. It would be advisable, initially, to do careful comparisons, in the same way as been done here, between the deformation theory and the incremental theory, in order to determine the range of usefulness of the former.

If the result obtained in the previous Section 3.6 can be extended to nonaxisymmetric stresses, which should not be too difficult where the full *in situ* stress field has been measured, it will be possible to infer a yield criterion for a homogeneous rock from extensometer measurements. It will obviously be more difficult to extend this to layered strata.

The challenge, then, for the successful application of the method is to develop a proper and consistent method of determining the input parameters for this and other numerical models. There is no doubt that this must incorporate some back-analysis of data obtained from monitored underground excavations in rock. This, combined with the laboratory testing and available rock mass classification schemes, should lead over the next decade to a greatly improved ability to model and design underground excavations where yield is an important factor.

3.8 APPENDIX: SOLUTION FOR AN ELASTIC RING BONDED TO A SEMIINFINITE MEDIUM

For simplicity we set $\phi^* = 0$. For a linear elastic ring j, where $r_j \leq r \leq r_{j+1}$, with modulus of elasticity E_j and Poisson's ratio v, the displacement, u, at r is given by

$$\frac{u}{r} = \left(\frac{1+v}{E_j}\right)\left\{p^*_{j+1}\left[1 - 2v + \frac{r_j^2}{r^2}\right] - p^*_j\left[(1-2v)\frac{r_j^2}{r_{j+1}^2} + \frac{r_j^2}{r^2}\right]\right\}\Big/\left(1 - \frac{r_j^2}{r_{j+1}^2}\right) \tag{74}$$

where p_j is the radial stress at $r = r_j$ and $p_j^* = p_j - \lambda_j p_0$ for λ_j given by equation (46) with E_s replaced by E_j.

The stresses are given by

$$\sigma_\theta = \left[p_{j+1}\left(1 + \frac{r_j^2}{r^2}\right) - p_j\left(\frac{r_j^2}{r_{j+1}^2} + \frac{r_j^2}{r^2}\right)\right]\Big/\left(1 - \frac{r_j^2}{r_{j+1}^2}\right) \tag{75a}$$

$$\sigma_r = \left[p_{j+1}\left(1 - \frac{r_j^2}{r^2}\right) - p_j\left(\frac{r_j^2}{r_{j+1}^2} - \frac{r_j^2}{r^2}\right)\right]\Big/\left(1 - \frac{r_j^2}{r_{j+1}^2}\right) \tag{75b}$$

$$\sigma_{r\theta} = 0 \tag{75c}$$

If the inner ring is ($r_1 \leq r \leq r_2$), we set $r_2 = r_e$ where r_e is given by equation (38) and $p_2 = p_e$ where p_e is given by equation (39). In the inner ring u is given by equation (74) with $j = 1$. With $j = 2$, $r_3 \to \infty$ and $p_3 = p_0$ we recover the expression (71) from equation (74) and expressions (35a–c) from equations (75a–c). Setting $r_1 = r_i$ and $p_1 = p_i$ to be consistent with previous notation, and using the expression for λ from equation (46)

$$\lambda p_0 = (E_1/E)p_0 + (1 - E_1/E)(p_e r_e^2/r_i^2 - p_i)/(r_e^2/r_i^2 - 1) \tag{76}$$

Equating u_e evaluated in the inner ring with the value obtained from equation (71) after some algebra gives

$$E_1/E = (p_e - p_i)/\{2(1-v)p_0(r_e^2/r_i^2 - 1) - p_e[2(1-v)r_e^2/r_i^2 - 1] + p_i(1-2v)\} \tag{77}$$

and the expression for u_i, the displacement at the opening boundary is

$$u_i/r_i = [(1+v)/E]/[2(1-v)(p_0 - p_e)r_e^2/r_i^2 - (1-2v)(p_0 - p_i)] \tag{78}$$

This expression has the interesting feature that the postfailure properties of the rock appear only through the r_e term (equation 38). Furthermore, this expression is identical to that obtained from the analytical solution in the case of ideal plasticity, a truly astonishing result!

ACKNOWLEDGEMENTS

Thanks are given to: Professors Bernard Budiansky, J. Lyell Sanders and J. W. Hutchinson for recent discussions at Harvard on the deformation theory of plasticity, as well as their dedicated and outstanding teaching 25 years ago; Hans Mühlhaus for many discussions and helpful suggestions; Michael Coulthard for doing the FLAC runs; Stuart Craig for helping with FESOFT runs and plots, for simplification of the axisymmetric solutions and also for helpful suggestions on the manuscript; and Chris Fama for setting up the macros for the type-setting software LaTeX for the submitted manuscript.

3.9 REFERENCES

1. Trueman R. A finite element analysis for the establishment of stress development in a coal mine caved waste. *Min. Sci. Tech.* **10**, 247–252 (1990).
2. Vermeer P. A. and Schotman G. J. M. An extension to the deformation theory of plasticity. In *Proc 2nd Int. Symp. Numer. Methods Geomech.*, Ghent (Edited by G. N. Pande and W. F. Van Impe), pp. 33–41. Jackson, Redruth (1986).
3. Wilson A. H. A method of estimating the closure and strength of lining required in drivages surrounded by a yield zone. *Int. J. Rock Mech. Min. Sci. & Geomech. Abstr.* **17**, 349–355 (1980).
4. Hoek E. and Brown E. T. *Underground Excavations in Rock*, pp. 14–37. Institution of Mining and Metallurgy, London (1980).
5. Bieniawski Z. T. Determining rock mass deformability: Experience from case histories. *Int. J. Rock Mech. Min. Sci. & Geomech. Abstr.* **15**, 237–247 (1978).
6. Follington I. L. and Isaac A. K. Failure zone development above longwall panels *Min. Sci. Tech.* **10**, 103–116 (1990).
7. Sakurai S. and Takeuchi K. Back analysis of measured displacements of tunnels. *Rock Mech. Rock Eng.* **16**, 173–180 (1983).
8. Hill R. *The Mathematical Theory of Plasticity*. Clarendon Press, Oxford (1950).
9. Kachanov L. M. *Fundamentals of the Theory of Plasticity*, Mir, Moscow (English Translation) (1974).
10. Hencky H. Zur Theorie plastischer Deformationen und der hierdurch im Material herforgerufenen Nachspannungen. *Z. Angew. Math. Mech.* **4**, 323–334 (1924).
11. Sanders J. L. Plastic stress–strain relations based on linear loading functions. In *Proc 2nd U.S. Natl. Congr. Appl. Mech.*, Ann Arbor, pp. 455–460. ASME, New York (1954).
12. Budiansky B. A re-assessment of deformation theories of plasticity. *J. Appl. Mech.* **26**, 259–264 (1959).
13. Detournay E. An approximate statical solution of the elastoplastic interface for the problem of Galin with a cohesive-frictional material. *Int. J. Solids Struct.* **22**, 1435–1454 (1986).
14. Vardoulakis I. and Graf B. Calibration of constitutive models for granular materials using data from biaxial experiments. *Geotechnique* **35**, 299–317 (1985).
15. Brown E. T., Bray J. W., Ladanyi B. and Hoek E. Ground response curves for rock tunnels. *J. Geotech. Eng.* **109**, 15–39 (1983).
16. Kripakov N. P. and Melvin M. T. A computer procedure to simulate progressive rock failure around coal mine entries. In *Proc. 1st Conf. Use of Computers in the Coal Industry*, Morgantown (Edited by Y. J. Wang and R. L. Sanford), pp. 487–502. SME, AIME, New York (1983).
17. Duncan Fama M. E. and Wardle L. J. Numerical analysis of coal mine chain pillar stability. In *Proc. 6th Int Congr. Rock. Mech.*, Montreal (Edited by G. Herget and S. Vongpaisal), pp. 859–863. Balkema, Rotterdam (1987).
18. Duncan Fama M. E. A new constitutive equation for a Coulomb material. In *Proc. ISRM Symp. Design and Performance of Underground Excavations*, Cambridge (Edited by E. T. Brown and J. A. Hudson), pp. 139–147. BGS, London (1984).
19. Florence A. L. and Schwer L. E. Axisymmetric compression of a Mohr–Coulomb medium around a circular hole. *Int. J. Numer. Anal. Methods Geomech.* **2**, 367–379 (1978).
20. Craig M. S. personal communication (1991).
21. Pender M. J., Graham C. J. and Gray W. J. Prefailure dilatancy and the stress distribution in a closely jointed rock mass. In *Proc. 5th Int Congr. Rock Mech.*, Melbourne, pp. C165–171. Balkema, Rotterdam (1983).
22. Duncan Fama M. E. and Craig M. S. FESOFT – A 2D finite element code with three degrees of freedom per node. *CSIRO Internal Report* No. 138 (1992).
23. FLAC – Fast Lagrangian Analysis of Continua, version 2.2 – User's Manual. Itasca Consulting Group, Inc., Minneapolis (1989).
24. Gale W. J. and Blackwood R. L. Stress distributions and rock failure around coal mine roadways. *Int. J. Rock Mech. Min. Sci. & Geomech. Abstr.* **24**, 165–173 (1987).
25. Gale W. J. Strata control utilising rock reinforcement techniques and stress control methods, in Australian coal mines. *The Mining Engineer* **150** (352), 247–253 (1991).
26. Beer G. An isoparametric joint-interface element for finite element analysis. *Int. J. Numer. Methods Eng.* **21**, 585–600 (1985).
27. Mühlhaus H.-B. and Vardoulakis I. The thickness of shear bands in granular materials. *Geotechnique* **37**, 271–283 (1987).
28. Mühlhaus H.-B. Lamination phenomena in pre-stressed rock. In *Proc. 2nd Int. Symp. Rockbursts and Seismicity in Mines*, Minneapolis, MN (Edited by C. Fairhurst), pp. 117–128. Balkema, Rotterdam (1990).
29. Kaiser P. K. A new concept to evaluate tunnel performance – influence of excavation procedure. In *Proc. 22nd U.S. Symp. Rock Mech.*, Cambridge, MA (Edited by H. H. Einstein), pp. 264–271. MIT Press, Cambridge, MA (1981).
30. Egger P. Deformations at the face of the heading and determination of the cohesion of the rock mass. *Underground Space* **4**, 313–318 (1980).